INTERNATIONAL JOURNAL FOR NUMERICAL METHODS IN ENGINEERING
Int. J. Numer. Meth. Engng 2004; **61**:142–155 (DOI: 10.1002/nme.1062)

Numerical analysis of a three-dimensional super-elastic constitutive model

Ferdinando Auricchio[1,2,*,†] and Ulisse Stefanelli[2,‡]

[1]*Dipartimento di Meccanica Strutturale, Università di Pavia, Via Ferrata, 1, I-27100 Pavia, Italy*
[2]*Istituto di Matematica Applicata e Tecnologie Informatiche - CNR, Italy*

SUMMARY

This note deals with the efficient approximation of a non-linear constitutive relation arising in the study of the three-dimensional mechanical behaviour of shape memory alloys at constant temperature. In particular, a variable time-step discretization is investigated. For such an algorithm we prove sharp error estimates of optimal order and exactness for a class of experimentally relevant situations. We also report numerical results relative to proportional and non-proportional loading tests which fully confirm the theoretical analysis. Copyright © 2004 John Wiley & Sons, Ltd.

KEY WORDS: shape-memory alloys; super-elasticity; hysteresis; discretization; error estimate

1. INTRODUCTION

The present paper focuses on the numerical approximation of a constitutive model, previously presented in the literature [1] and able to describe, with some simplifications, the three-dimensional super-elastic behaviour of shape-memory alloys in a small deformation realm. In particular, we investigate a variable time-step discretization, proving stability, convergence and sharp *a priori* error bounds of optimal order. To our knowledge this is the first contribution addressing an accurate numerical analysis in a three-dimensional framework for such a class of materials. Accordingly, we refer to the cited reference [1] or to other related references [2, 3] for a deeper and more material-oriented discussion on the model here investigated as well as to classical references [4–7] for a general description on shape-memory materials as well as on the related micro- and macro-scale phenomena. Therefore, we now start directly from the set of constitutive equations.

*Correspondence to: Ferdinando Auricchio, Dipartimento di Meccanica Strutturale, Università di Pavia, Istituto di Matematica Applicata e Tecnologie Informatiche - CNR, Via Ferrata, 1, I-27100 Pavia, Italy.
†E-mail: auricchio@unipv.it
‡E-mail: ulisse@imati.cnr.it

Received 9 July 2003
Published online 15 July 2004 *Revised 15 January 2004*
 Accepted 15 January 2004

The model under investigation is constructed from the basic assumption that the martensitic phase transition mechanism is associated to an always active reorientation process, described through the following equation:

$$\boldsymbol{\varepsilon}^{\mathrm{tr}} = \varepsilon_L \xi \frac{\partial F(\boldsymbol{\sigma})}{\partial \boldsymbol{\sigma}} \tag{1}$$

where $\boldsymbol{\varepsilon}^{\mathrm{tr}}$ is the inelastic strain induced by the martensitic transformation (in the following briefly indicated as *transformation strain*), ε_L is a positive material constant representing a measure of the maximum strain obtainable through alignment of the martensite variants, ξ is the martensite volume fraction, F is a loading function driving the phase transformation process and depending on the stress $\boldsymbol{\sigma}$.

To describe a different material response between traction and compression, we assume a loading function of Drucker–Prager type

$$F(\boldsymbol{\sigma}) := \|\mathbf{s}\| + 3\alpha p \tag{2}$$

with $\|\cdot\|$ the usual norm in the space $\mathbf{S}$ of symmetric and deviatoric tensors (i.e $\|\mathbf{s}\|^2 = \mathbf{s} : \mathbf{s}$), α a material parameter, while $\mathbf{s}$ and p are the deviatoric and the volumetric part of the stress, defined, respectively, as

$$\mathbf{s} := \boldsymbol{\sigma} - \left(\frac{\boldsymbol{\sigma} : \mathbf{1}}{3}\right)\mathbf{1} \tag{3}$$

$$p := \frac{\boldsymbol{\sigma} : \mathbf{1}}{3} \tag{4}$$

such that

$$\boldsymbol{\sigma} = \mathbf{s} + p\mathbf{1} \tag{5}$$

As classically done in the literature we introduce also the assumption of isotropic linear elastic response [8, 9] such that the model under investigation can be now written as

$$p = K(\theta - \theta^{\mathrm{tr}}) \tag{6}$$

$$\mathbf{s} = 2G(\mathbf{e} - \mathbf{e}^{\mathrm{tr}}) \tag{7}$$

$$\theta^{\mathrm{tr}} = 3\varepsilon_L \xi \alpha \tag{8}$$

$$\mathbf{e}^{\mathrm{tr}} = \varepsilon_L \xi \frac{\mathbf{s}}{\|\mathbf{s}\|} \tag{9}$$

$$\xi = g(\xi^0, F(\boldsymbol{\sigma})) \tag{10}$$

where

- K is the bulk modulus, while θ and θ^{tr} are the volumetric components of the strain $\boldsymbol{\varepsilon}$ and of the transformation strain $\boldsymbol{\varepsilon}^{\mathrm{tr}}$, defined, respectively, as

$$\theta := (\boldsymbol{\varepsilon} : \mathbf{1}) \quad \text{and} \quad \theta^{\mathrm{tr}} := (\boldsymbol{\varepsilon}^{\mathrm{tr}} : \mathbf{1}) \tag{11}$$

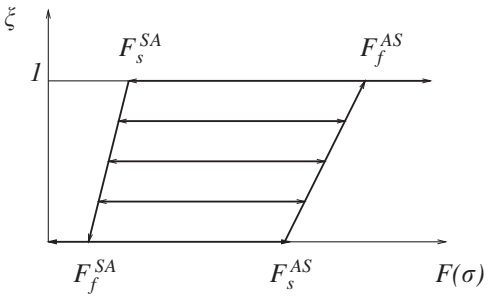

Figure 1. Diagram of relation g, expressing the dependency of the material fraction ξ on the general loading function $F(\boldsymbol{\sigma})$. The quantities F_{s}^{AS}, F_{f}^{AS}, F_{s}^{SA}, F_{f}^{SA} are material-dependent parameters.

- G is the shear modulus, while $\mathbf{e}$ and $\mathbf{e}^{\mathrm{tr}}$ are the deviatoric components of the strain $\boldsymbol{\varepsilon}$ and of the transformation strain $\boldsymbol{\varepsilon}^{\mathrm{tr}}$, defined, respectively, as

$$\mathbf{e} := \boldsymbol{\varepsilon} - \frac{\theta}{3}\mathbf{1} \quad \text{and} \quad \mathbf{e}^{\mathrm{tr}} := \boldsymbol{\varepsilon}^{\mathrm{tr}} - \frac{\theta^{\mathrm{tr}}}{3}\mathbf{1} \tag{12}$$

  Clearly, relation (9) is valid only for the case $\mathbf{s} \neq \mathbf{0}$, while for the case $\mathbf{s} = \mathbf{0}$ we set $\mathbf{e}^{\mathrm{tr}} = \mathbf{0}$.
- g is a non-linear relation expressing the dependency of the martensite fraction ξ on the stress $\boldsymbol{\sigma}$, through a generic loading function F, take in the following as the Drucker–Prager function defined in (2). A possible behaviour for the non-linear relation g is depicted in Figure 1.

We wish to stress that g is not a pointwise one-to-one relation and that it shall be actually interpreted as a hysteresis operator; namely, it is fundamentally non-local in time. Indeed, as evident from Figure 1 the quantity $\xi(t)$ is not defined from $F(\boldsymbol{\sigma}(t))$ itself but it also depends on the past history of $F(\boldsymbol{\sigma})$ over the time range $[0, t]$. We conclude by observing that the above comments will be soon made precise from the mathematical viewpoint once a proper description of g is provided (see (16)).

However, before proceeding with the mathematical discussion on the model, it is important to make the following remarks:

- As commented in Reference [1], Equation (1) implies an always-active reorientation process for the martensite variants, which constitutes an approximation from the physical and the dissipative thermo-mechanical modelling perspective. Accordingly, this position implies that for positive values of the martensite fraction ξ the transformation strain $\boldsymbol{\varepsilon}^{\mathrm{tr}}$ varies continuously with $\partial F(\boldsymbol{\sigma})/\partial\boldsymbol{\sigma}$. This condition is particularly effective in the case of non-proportional loading regimes.
- Dealing from now on with a loading function of Drucker–Prager type (2), as discussed in Reference [3], we can easily relate the material parameter α and the significative points of the relation g, i.e. F_{s}^{AS}, F_{f}^{AS}, F_{s}^{SA}, F_{f}^{SA}, to quantities with a more clear physical role indicated as

$$\sigma_{\mathrm{s}}^{AS,+},\ \sigma_{\mathrm{f}}^{AS,+},\ \sigma_{\mathrm{s}}^{SA,+},\ \sigma_{\mathrm{f}}^{SA,+},\ \sigma_{\mathrm{s}}^{AS,-}$$

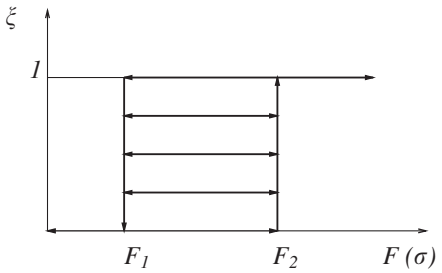

Figure 2. Diagram of relation g, expressing the dependency of the material fraction ξ on the general loading function $F(\boldsymbol{\sigma})$, for the case of no hardening.

The latter quantities represent, respectively, the start and final value for the austenite-martensite conversion in traction, the start and final value for the martensite–austenite conversion in traction, the start value for the austenite–martensite conversion in compression (see the forthcoming Section 4).

As a final comment, we wish to observe that we are in the position of considering also the limiting case

$$F_{\mathrm{s}}^{SA} = F_{\mathrm{f}}^{SA} = F_1, \quad F_{\mathrm{s}}^{AS} = F_{\mathrm{f}}^{AS} = F_2$$

(Figure 2) which actually corresponds to the situation without hardening. The latter situation is indeed the most interesting from the mathematical point of view since the bounding curves of the hysteretic region in Figure 1 turn out to be multivalued applications with vertical segments. For the sake of notational simplicity we shall stick to this case for the rest of the paper.

Of course, starting from the current choice of g, the interested reader may extend our argument to the previously introduced general case without any particular difficulty.

2. MATHEMATICAL FORMULATION

We shall collect in this section some details on the mathematical treatment of model (6)–(10). First of all, we shall rewrite the problem in a more compact form. Indeed, assuming $\boldsymbol{\varepsilon}$ to be given for all times, we observe that, in order to find a solution to (6)–(10), it suffices to determine the evolution of the phase proportion ξ. Let us now exploit the particular structure of (7)–(9), and deduce that

$$\|\mathbf{s}\| = 2G\|\mathbf{e} - \mathbf{e}^{\mathrm{tr}}\| = 2G(\|\mathbf{e}\| - \varepsilon_L \xi)$$

Hence, owing to (2), (6) and (8), we readily have that

$$F(\boldsymbol{\sigma}) = (2G\|\mathbf{e}\| + 3\alpha K\theta) - \varepsilon_L(2G + 9\alpha^2 K)\xi$$

In particular, the parallelism of $\mathbf{s}$ and $\mathbf{e}^{\mathrm{tr}}$ stated in (9) suggests the reduction of the model to a scalar analogue. Namely, we relate the scalar output ξ to the scalar datum

$$e := 2G\|\mathbf{e}\| + 3\alpha K\theta$$

and rewrite relation (10) as

$$\xi = q(\xi^0, e) \tag{13}$$

where q, setting the positive constant $\mu := \varepsilon_L(2G + 9\alpha^2 K)$, is the relation depicted below:

Hysteretic relations of type (13) are usually called *generalized play-type operators* and the interested reader is referred to References [10–12] for a full discussion on this kind of hysteretic relations together with a variety of possible generalizations. For the sake of clarity, we just want to state some detail on the mathematical notion of hysteresis operator. Let $C[0, T]$ denote the space of continuous real-valued functions. We say that $H : C[0, T] \to C[0, T]$ is a *hysteresis operator* if and only if

- it is *causal*, i.e. for any $u, v \in C[0, T]$ such that $u = v$ on $[0, t]$ for some $t \in [0, T]$ we have that $H[u] = H[v]$ on $[0, t]$ as well (the square brackets are used in order to stress the *functional dependence*),
- it is *rate independent*, namely given any increasing homeomorphism $s : [0, T] \longrightarrow [0, T]$, the following relation holds:

$$H[u \circ s](t) = H[u](s(t)) \quad \forall t \in [0, T]$$

The latter rate independence condition ensures that the value of the output is independent from the speed at which the input attains its values. This is indeed a typical feature of hysteretic phenomena.

Our next aim is to rewrite relation (13) as an evolution equation for ξ. In fact, whenever an absolutely continuous input e is considered, we may provide a completely equivalent differential formulation for (13). However, since q is not a pointwise one-to-one relation, the differential formulation corresponding to (13) is not obtained by a simple differentiation in time [2].

First of all we introduce the two piecewise affine functions $\lambda_\ell, \lambda_u : \mathbb{R} \longrightarrow [0, 1]$ as

$$\lambda_\ell(r) := \max\{0, \min\{1, (r - F_2)/\mu\}\} \tag{14}$$

$$\lambda_u(r) := \max\{0, \min\{1, (r - F_1)/\mu\}\} \tag{15}$$

The latter are exactly the lower and upper bounds of the hysteretic region $E \subset \mathbb{R}^2$ in Figure 3. Then, let $K : \mathbb{R} \longrightarrow 2^{\mathbb{R}}$ be the *set-valued* function

$$K(r) := [\lambda_\ell(r), \lambda_u(r)] \quad \forall r \in \mathbb{R}$$

(hence $E = \text{graph } K$). Now we shall introduce, for any $r \in \mathbb{R}$, the indicator function $I_{K(r)}$ of the non-empty, bounded, and closed interval $K(r)$, namely

$$I_{K(r)}(y) = 0 \quad \text{if } y \in K(r) \quad \text{and} \quad I_{K(r)}(y) = +\infty \text{ otherwise}$$

Let us recall that the above function is convex, proper and lower semicontinuous for any $r \in \mathbb{R}$. Finally, we denote by $\partial I_{K(r)} : [0, 1] \longrightarrow 2^{\mathbb{R}}$ the *subdifferential* of $I_{K(r)}$. This is the *set-valued function*

$$x \in \partial I_{K(r)}(y) \Longleftrightarrow y \in K(r) \quad \text{and} \quad x(w - y) \leqslant 0 \quad \forall w \in K(r)$$

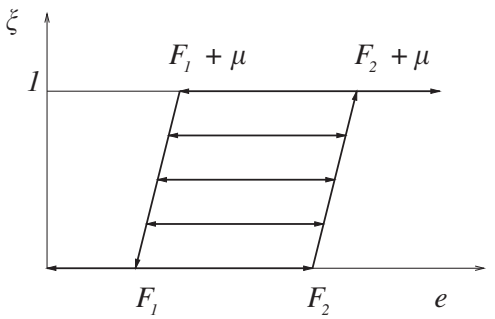

Figure 3. Diagram of relation q, expressing the dependency of the material fraction ξ on the strain measure e.

In our specific case, one has that

$$\partial I_{K(r)}(y) := \begin{cases} 0 & \text{if } \lambda_\ell(r) < y < \lambda_u(r) \\ [0, +\infty) & \text{if } y = \lambda_u(r) \\ (-\infty, 0] & \text{if } y = \lambda_\ell(r) \\ \emptyset & \text{otherwise} \end{cases}$$

Of course the latter multi-valued operator is of *maximal monotone type* in $\mathbb{R} \times \mathbb{R}$ and the reader is referred to Reference [13] for details.

We are now in the position of claiming that (13) may be reformulated as the initial value problem

$$\dot{\xi}(t) + \partial I_{K(e(t))}(\xi(t)) \ni 0 \quad \text{for a.e. } t \in (0, T), \quad \xi(0) = \xi^0 \tag{16}$$

which, owing to the above discussion, is of course equivalent to the *variational inequality* for almost every $t \in (0, T)$,

$$\xi(t) \in K(e(t)) \quad \dot{\xi}(t)(\xi(t) - w) \leqslant 0 \quad \forall w \in K(e(t)) \tag{17}$$

together with the initial condition of (16).

In order to clarify the latter claim, we observe that relation (16) is completely equivalent to the following set of conditions:

$$\lambda_\ell(e) \leqslant \xi \leqslant \lambda_u(e) \quad \text{a.e. in } (0, T)$$

$$\dot{\xi} = 0 \quad \text{a.e. on the set } \{\lambda_\ell(e) < \xi(t) < \lambda_u(e)\}$$

$$\dot{\xi} \geqslant 0 \quad \text{a.e. on the set } \{\xi = \lambda_\ell(e)\}$$

$$\dot{\xi} \leqslant 0 \quad \text{a.e. on the set } \{\xi = \lambda_u(e)\}$$

which is exactly the non-linear relation depicted in Figure 3.

We shall now conclude this section by stating a well-posedness result for the continuous model (16), referring to Reference [14] for definitions and details on Sobolev spaces.

Lemma 2.1
Assume $e \in H^1(0,T)$ and $\xi^0 \in K(e(0))$. Then there exists a unique function $\xi \in H^1(0,T)$ fulfilling (16).

A proof of the latter lemma can be essentially found in Reference [12, Theorem 2.3, p. 67].

3. DISCRETIZATION

Let us now focus on a possible approximation for (16). We are interested in a *variable time-step discretization* of the problem. The aim is to introduce an algorithm in order to compute step-by-step the phase proportion starting from a suitable approximation of the datum e.

Let us start by introducing the partition

$$\mathscr{P} := \{0 = t_0 < t_1 < \cdots < t_{N-1} < t_N = T\}$$

with variable time step $\tau_i := t_i - t_{i-1}$ and let $\tau := \max_{1 \leqslant i \leqslant N} \tau_i$ denote the diameter of the partition $\mathscr{P}$. No constraints are imposed on the possible choice of the time steps.

In the forthcoming analysis, the following notation will be extensively used: being $\{u_i\}_{i=0}^N$ a vector, we denote by $u_\mathscr{P}$ and $\bar{u}_\mathscr{P}$ two functions of the time interval $[0,T]$ which interpolate the values of the vector $\{u_i\}$ piecewise linearly and backward constantly on the partition $\mathscr{P}$, respectively. Namely

$$u_\mathscr{P}(0) := u_0, \quad u_\mathscr{P}(t) := \alpha_i(t)u_i + (1 - \alpha_i(t))u_{i-1}$$

$$\bar{u}_\mathscr{P}(0) := u_0, \quad \bar{u}_\mathscr{P}(t) := u_i \quad \text{for } t \in (t_{i-1}, t_i], \ i = 1, \ldots, N$$

where

$$\alpha_i(t) := \frac{t - t_{i-1}}{\tau_i} \quad \text{for } t \in (t_{i-1}, t_i], \ i = 1, \ldots, N$$

Finally, we indicate with $e_\mathscr{P}$ and $\xi^0_\mathscr{P}$ suitable approximations of e and ξ^0, fulfilling the compatibility condition $\xi^0_\mathscr{P} \in K(e_\mathscr{P}(0))$. In particular, let us stress that the standard choice from the experimental point of view is

$$e_i := e(t_i) \quad \text{for } i = 0, 1, \ldots, N, \ \ \xi^0_\mathscr{P} := \xi^0 \tag{18}$$

In the latter situation, the compatibility condition on the initial data is fulfilled whenever the assumptions of Lemma 2.1 hold. Nevertheless, we are obviously in the position of providing a somehow more general approximation result.

We are interested in the following discrete scheme:

$$\xi_0 = \xi^0_\mathscr{P}, \quad \frac{\xi_i - \xi_{i-1}}{\tau_i} + \partial I_{K(e_i)}(\xi_i) \ni 0 \quad \text{for } i = 1, \ldots, N \tag{19}$$

Of course the problem of finding a suitable $\{\xi_i\}_{i=0}^N \in \mathbb{R}^{N+1}$ fulfilling (19) is well-posed. Indeed, we remark that ξ_i is *explicitly computable* from ξ_{i-1} and e_i as

$$\xi_i = \pi_{K(e_i)}(\xi_{i-1}) := \min\{\lambda_u(e_i), \max\{\xi_{i-1}, \lambda_\ell(e_i)\}\} \tag{20}$$

where $\pi_{K(e_i)}$ denotes the projection on the non-empty, convex and closed set $K(e_i)$. It is worth noting that the latter algorithm (20) is completely analogous to the well-known *return mapping algorithm* in plasticity. As a matter of fact we are exploiting a similar idea in order to cope with the *pseudo-plastic* behaviour of a shape memory alloy, adapting indeed the procedure to the case of as *time-dependent yield criterion*. We conclude our discussion on the algorithm by observing the time step τ_i does not appear in equality (20). This fact is the discrete analogue of the *rate independence* [12] of relation q in the sense discussed in the previous section.

Owing to the latter considerations and making indeed use of the above-introduced notation we may equivalently rewrite (19) in the more compact form as

$$\dot{\bar{\xi}}_{\mathscr{P}}(t) + \partial I_{K(\bar{e}_{\mathscr{P}}(t))}(\bar{\xi}_{\mathscr{P}}(t)) \ni 0 \quad \text{for a.e. } t \in (0, T), \qquad \xi_{\mathscr{P}}(0) = \xi^0_{\mathscr{P}} \tag{21}$$

We state without proof the following trivial *stability* result

Lemma 3.1
The solution to (21) fulfils $|\dot{\bar{\xi}}_{\mathscr{P}}| \leqslant |\dot{e}_{\mathscr{P}}|/\mu$ on $(0, T)$.

As for the convergence of the solution $\xi_{\mathscr{P}}$ to the discrete scheme (21) to a solution ξ of (16) we shall start from the following lemma that indeed states a *continuous dependence on data* for problem (16).

Lemma 3.2
Let $e_j, \xi_j \in H^1(0, T)$ fulfil (16) for $j = 1, 2$. Then, for any $t \in [0, T]$,

$$|(\xi_1 - \xi_2)(t)| \leqslant \max\{|(\xi_1 - \xi_2)(0)|, \max_{s\in[0,t]} |(e_1 - e_2)(s)|/\mu\}$$

The proof of the latter result is contained in Reference [12, Lemma 2.1, p. 66 and Theorem 2.2, p. 67]. It is interesting to stress that the latter estimate is sharp, since it reduces to an equality for some choice of $\xi_i(0), e_i$ for $i = 1, 2$ (e.g. let $\xi_1(0) = \xi_2(0) = 0$, $e_1(t) = F_2 = e_2(t) - t$, and $T = \mu$).

On the other hand, let $\zeta_{\mathscr{P}} \in H^1(0, T)$ be the solution to (16) with initial datum $\zeta_{\mathscr{P}}(0) = \xi^0_{\mathscr{P}}$ and $e = e_{\mathscr{P}}$. Of course, since $e_{\mathscr{P}}$ is piecewise affine on $\mathscr{P}$ by definition, the function $\zeta_{\mathscr{P}}$ turns out to be piecewise affine as well. Moreover, it is a trivial matter to check that

$$\zeta_{\mathscr{P}}(t_i) \equiv \xi_{\mathscr{P}}(t_i) \quad \text{for } i = 0, 1, \ldots, N$$

hence, we readily get that

$$\max_{t\in[0,T]} |(\xi_{\mathscr{P}} - \zeta_{\mathscr{P}})(t)| \leqslant \tau/(4\mu) \tag{22}$$

where the latter bound is sharp (this is indeed a straightforward computation).

We are now in the position of stating the following *convergence and error estimate* result

Lemma 3.3
Under the above assumptions and notations we have that, for any $t \in [0, T]$ and $i = 0, 1, \ldots, N$,

$$\max_{s\in[0,t]} |(\xi - \xi_{\mathscr{P}})(s)| \leqslant \max\left(|\xi^0 - \xi^0_{\mathscr{P}}|, \max_{s\in[0,t]} |(e - e_{\mathscr{P}})(s)|/\mu\right) + \tau/(4\mu) \tag{23}$$

$$|(\xi - \xi_{\mathscr{P}})(t_i)| \leqslant \max\left(|\xi^0 - \xi^0_{\mathscr{P}}|, \max_{s\in[0,t_i]} |(e - e_{\mathscr{P}})(s)|/\mu\right) \tag{24}$$

Proof
Apply Lemma 3.2 with the choices $\xi_1 = \xi$ and $\xi_2 = \zeta_{\mathscr{P}}$ taking into account (22).

In order to give a concrete example of the latter error control we turn to the experimental standard case of (18) and specialize Lemma 3.3 in the following result.

Corollary 3.4
Let $e \in W^{1,\infty}(0, T)$, $\xi^0 \in K(e(0))$, and (18) hold. Then

$$\max_{t\in[0,T]} |(\xi - \xi_{\mathscr{P}})(t)| \leqslant (\|\dot{e}\|_{L^\infty(0,T)} + 1/(4\mu))\tau \tag{25}$$

Proof
It suffices to exploit (23) and compute, for $t \in (t_{i-1}, t_i]$, $i = 1, \ldots, N$,

$$\begin{aligned} |(e - e_{\mathscr{P}})(t)| &= |\alpha(t)(e(t) - e(t_i)) + (1 - \alpha(t))(e(t) - e(t_{i-1}))| \\ &\leqslant \int_{t_{i-1}}^{t_i} |\dot{e}(s)|\,\mathrm{d}s \leqslant \tau\|\dot{e}\|_{L^\infty(0,T)} \end{aligned} \tag{26}$$

The latter *a priori estimates* of the discretization error are *optimal* with respect to the order of convergence, since we used the first-order Euler's method to approximate the time derivative in (16). Then, it is clear that the above estimates are *sharp* in the sense that the inequalities in (23)–(24) actually reduce to equalities in some particular case. Moreover, no constraint are imposed on the possible choice of time steps throughout the analysis. In particular, the latter time steps can be tailored according to other possible experimental or numerical considerations.

The *pointwise* estimate (24) claims that, whenever $\xi^0 = \xi^0_{\mathscr{P}}$ and e is piecewise affine (this is indeed the case of most experimental situations) the scheme solves the problem without error on $\mathscr{P}$ (provided that $\mathscr{P}$ includes the discontinuity points of $\dot{e}$, of course). Namely, we have the following.

Corollary 3.5
Let e be piecewise affine on $\mathscr{P}$ and (18) hold. Then $\xi = \xi_{\mathscr{P}}$ on $\mathscr{P}$. Namely, the algorithm solves the problem without error.

Remark 3.6
A variety of possibly alternative error estimates can be obtained by playing with the variational inequalities (16) and (21). Indeed, we limit ourselves to (23)–(24) just for the sake of clarity. Let us just observe that the same conclusion of Corollary 3.5 holds indeed also in the case of a piecewise monotone datum e as well.

Remark 3.7
The main part of the above stated results hold under a number of interesting generalizations with minor modifications. In particular the latter analysis can be easily adapted to the case of Lipschitz continuous functions $\lambda_\ell \leqslant \lambda_u$ as well as to more general set-valued functions K even in the multidimensional case.

4. NUMERICAL EXAMPLES

In the following, we provide numerical evidences on the effectiveness of the algorithm proposed in (20). Clearly, the time discrete scheme for the computation of ξ_i is coupled with the remaining part of the model, i.e. with Equations (6)–(9). We also note that it is easy to compute the tangent consistent with the proposed algorithm; however, for brevity, we do not report the steps for its derivation.

As numerical examples we consider a uniaxial tension test as well as three biaxial non-proportional tests. For the uniaxial tension test, the loading is imposed assuming to control one strain component and requiring that all the other stress components are identically equal to zero, while for the biaxial tests the loading is imposed assuming to control two strain components and requiring that all the stress components not corresponding to the two controlled strains are identically equal to zero. In particular, in the three biaxial problems we control the following strain components:

$$\text{Biaxial tension: } \varepsilon_{11}\ \varepsilon_{22}$$

$$\text{Biaxial torsion: } \varepsilon_{12}\ \varepsilon_{23}$$

$$\text{Tension torsion: } \varepsilon_{11}\ \varepsilon_{12}$$

Figure 4 reports the load history for the uniaxial tension test in terms of strain component versus time, while Figure 5 reports the load history for the biaxial tension test in terms of strain ε_{11} versus strain ε_{22}; the loading histories for the other two biaxial tests are not reported since they can be obtained simply changing the indices for the controlled strain components.

The material elastic response is described through the two constants:

$$E = 70000\,\text{MPa} \quad \text{and} \quad v = 0.33 \tag{27}$$

where Young's modulus E and Poisson's ratio v uniquely determine the constants

$$K = \frac{E}{3(1-2v)} \quad \text{and} \quad G = \frac{E}{2(1+v)} \tag{28}$$

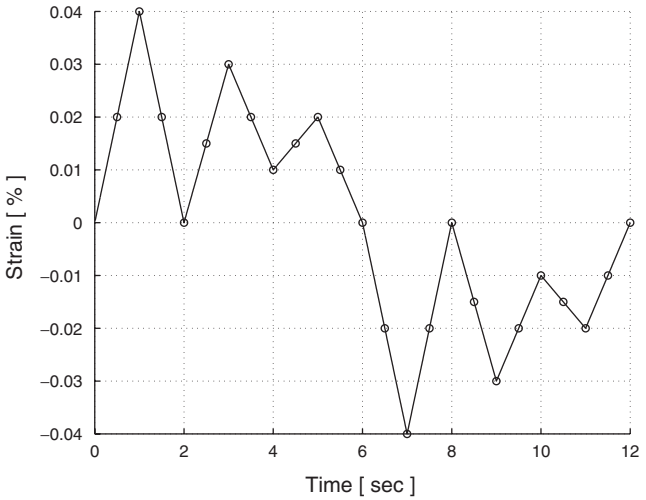

Figure 4. Uniaxial tension test: loading history in terms of strain versus time for two different time discretizations.

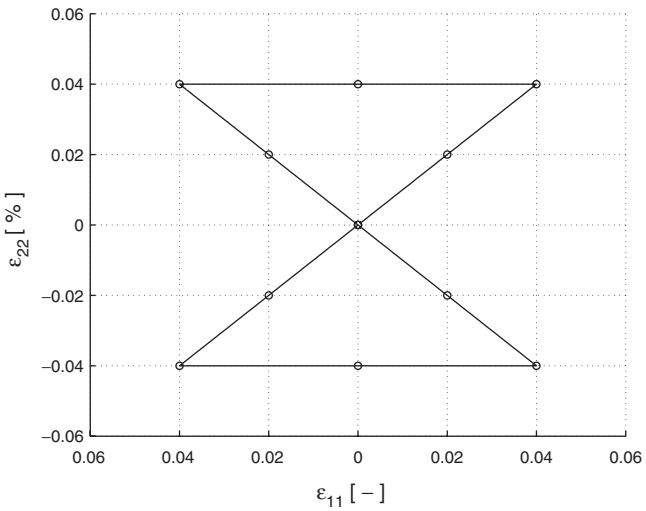

Figure 5. Biaxial test: loading history (in terms of strain ε_{11} versus strain ε_{22}) for two different time discretizations.

The material inelastic response is described through the following constants:

$$\sigma_{\mathrm{s}}^{AS,+} = 500\ \mathrm{MPa} \quad \sigma_{\mathrm{f}}^{AS,+} = 500\ \mathrm{MPa}$$

$$\sigma_{\mathrm{s}}^{SA,+} = 200\ \mathrm{MPa} \quad \sigma_{\mathrm{f}}^{SA,+} = 200\ \mathrm{MPa}$$

$$\sigma_{\mathrm{s}}^{AS,-} = 700\ \mathrm{MPa} \quad \varepsilon_L = 0.03$$

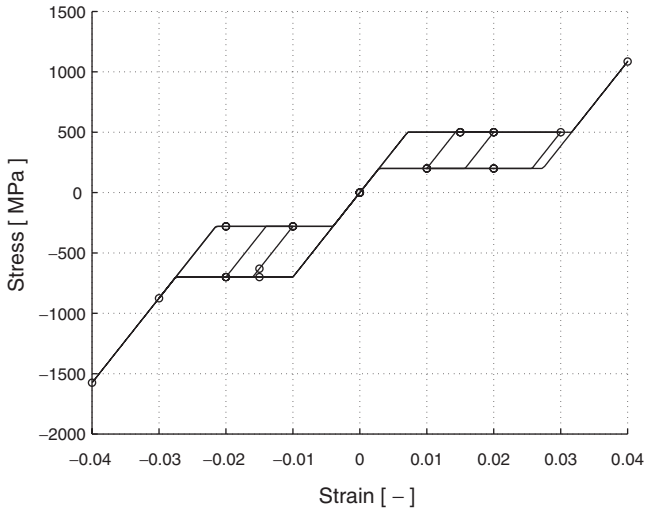

Figure 6. Uniaxial tension test: numerical results (in terms of stress versus strain) for two different time discretizations.

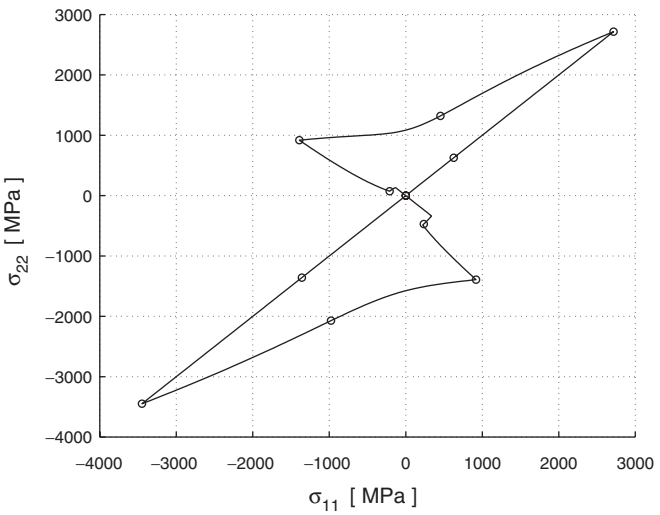

Figure 7. Biaxial tension test: numerical results (in terms of stress σ_{11} versus stress σ_{22}) for two different time discretizations.

and, following Reference [1], we can compute the parameter α

$$\alpha = \frac{\sigma_{\mathrm{s}}^{SA,-} - \sigma_{\mathrm{s}}^{SA,+}}{\sigma_{\mathrm{s}}^{SA,-} + \sigma_{\mathrm{s}}^{SA,+}} \tag{29}$$

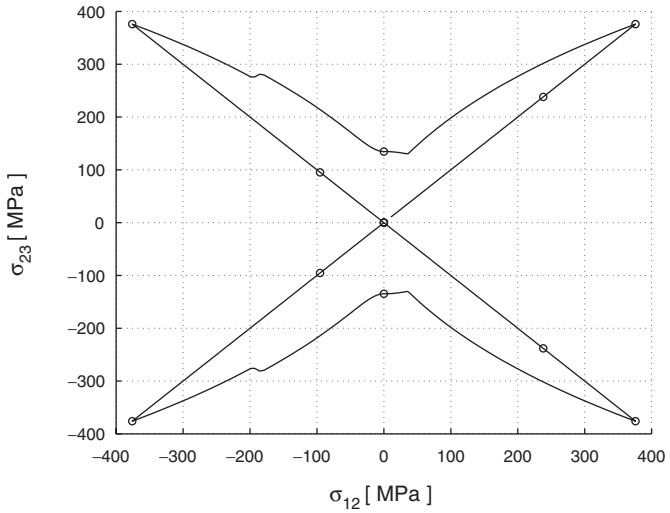

Figure 8. Biaxial torsion test: numerical results (in terms of stress σ_{12} versus stress σ_{23}) for two different time discretizations.

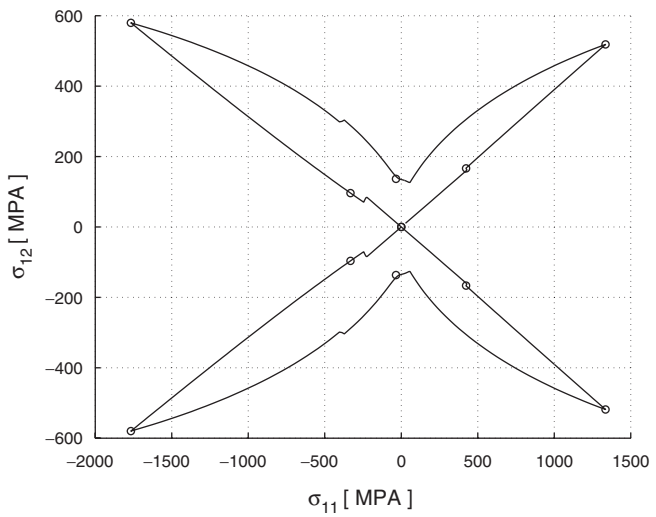

Figure 9. Tension torsion test: numerical results (in terms of stress σ_{11} versus stress σ_{12}) for two different time discretizations.

Lacking the analytic solution of the problems under investigation, we computed the numerical solutions with a very fine time interval, corresponding to 100 steps per second [$\mathrm{d}t = 0.01$ s] and with a very large time interval, corresponding to 2 steps per second [$\mathrm{d}t = 0.5$ s]. Figures 6–9 report the results for the different loading histories and for the two time discretizations. It is worth to point out how also for the extremely crude time approximation we obtain exact pointwise numerical solutions, in accordance with Corollary 3.5.

REFERENCES

1. Auricchio F, Taylor RL, Lubliner J. Shape-memory alloys: macromodelling and numerical simulations of the superelastic behaviour. *Computer Methods in Applied Mechanics and Engineering* 1997; **146**:281–312.
2. Auricchio F, Taylor RL. Shape-memory alloys: modelling and numerical simulations of the finite-strain superelastic behaviour. *Computer Methods in Applied Mechanics and Engineering* 1997; **143**:175–194.
3. Auricchio F. A robust integration-algorithm for a finite-strain shape-memory-alloy superelastic model. *International Journal of Plastics* 2001; **17**:971–990.
4. Duerig TW, Melton KN, Stockel D, Wayman CM (eds). Engineering Aspects of Shape Memory Alloys. Butterworth-Heinemann: London, 1990.
5. Wayman CM, Duerig TW. An introduction to martensite and shape memory. In *Engineering Aspects of Shape Memory Alloys*, Duerig TW, Melton KN, Stockel D, Wayman CM (eds). 1990; 3–20.
6. Wayman CM. Shape memory and related phenomena. *Progress in Material Science* 1992; **36**:203–224.
7. Wayman CM. Shape memory alloys. *MRS Bulletin*, April, 1993; 49–56.
8. Raniecki B, Lexcellent C. R_L-models of pseudoelasticity and their specification for some shape memory solids. *European Journal of Mechanics – A/Solids* 1994; **13**:21–50.
9. Souza AC, Mamiya EN, Zouain N. Three-dimensional model for solids undergoing stress-induced phase transformations. *European Journal of Mechanics – A/Solids* 1998; **17**:789–806.
10. Brokate M, Sprekels J. *Hysteresis and Phase Transitions*. Applied Mathematical Sciences, vol. 121. Springer: Berlin, 1996.
11. Krasnosel'skiĭ MA, Pokrovskiĭ AV. *Systems with Hysteresis*. Springer-Verlag: Berlin, 1989 (Translated from Russian by Marek Niezgódka).
12. Visintin A. *Differential Models of Hysteresis*, Applied Mathematical Sciences, vol. 111. Springer: Berlin, 1994.
13. Brezis H. *Opérateurs Maximaux Monotones et Semi-groupes de Contractions dans les Espaces de Hilbert*, North Holland Mathematics Studies, vol. 5. North-Holland: Amsterdam, 1973.
14. Lions J-L. Magenes E. *Non-homogeneus Boundary Value Problems and Applications*, vol. 1. Springer, New York, Heidelberg, 1972.

